

# A fully automatic curve localization method for extracted spine

Aishu Xie<sup>1,2,3</sup>, Ervin Gubin Mounq<sup>2</sup>, Xu Zhou<sup>4</sup>, Zhibang Yang<sup>5</sup>

<sup>1</sup>Faculty of Computer and Artificial Intelligence, Huai Hua University, Huai Hua, China

<sup>2</sup>Faculty of Computing and Informatics, Universiti Malaysia Sabah, Sabah, Malaysia

<sup>3</sup>Key Laboratory of Wuling-Mountain Health Big Data Intelligent Processing and Application in Hunan Province Universities, Huai Hua, China

<sup>4</sup>College of Computer Science and Electronic Engineering, Hunan University, Changsha, China

<sup>5</sup>Key Laboratory of Industrial Internet Technology and Security in Hunan Province, Changsha University, Changsha, China

## Article Info

### Article history:

Received Feb 13, 2024

Revised Apr 25, 2024

Accepted Apr 30, 2024

### Keywords:

Adapted distance transform

Curve type

Line segment searching

Line sequence

Quadratic line fitting

Scoliosis positioning

## ABSTRACT

The automation of scoliosis positioning presents a challenging and often understated task, yet it holds fundamental significance for the automated analysis of spinal morphological anomalies. This paper introduces a novel spinal curve localization model for precisely differentiating the spinal curves and identifying their concave centers. The proposed model contains three components: i) custom spine central line model, to define the spine central line as a combination of several secant line sequences with different polarities; ii) custom curve model, to classify each spinal curve into one of 11 curves types and deduce each its concave centers by several custom formulas; and iii) adapted distance transform and quadratic line fitting algorithm coupled with custom secant line segment searching strategy (DTQL-LS), to search all line segments in the spine and group consecutive line segments with identical polarity into line sequence. Experimental results show that its positioning success rate is close to 99%. Furthermore, it exhibits significant time efficiency, with the average time to process a single image being less than 30 milliseconds. Moreover, even if some image boundaries are blurred, the center of the curve can still be accurately located.

This is an open access article under the [CC BY-SA](https://creativecommons.org/licenses/by-sa/4.0/) license.



## Corresponding Author:

Ervin Gubin Mounq

Faculty of Computing and Informatics, Universiti Malaysia Sabah

UMS 884400 street, Kota Kinabalu, Sabah, Malaysia

Email: ervin@ums.edu.my

## 1. INTRODUCTION

Scoliosis is a deformation of the spinal column and its pathogenesis has not been completely elucidated to date. According to the statistics, the incidence of adolescent idiopathic scoliosis (AIS) is approximately 1%-3% [1], [2], and the morbidity of congenital scoliosis (CS) of infants is approximately 0.5%-1% [3]. If allowed to progress, it may lead to irreversible deformities in the patient's physique and even trigger additional complications. Therefore, regular nationwide screening and assessment for scoliosis among adolescents are imperative, and for people who have been diagnosed with scoliosis, it is also necessary to track and monitor the patient's condition through regular examinations so that the optimal diagnosis and treatment plan can be adjusted timely.

The measurement of spinal curvature primarily involves assessing the degree of curvature in the three regions: cervical-thoracic, main thoracic, and thoracic-lumbar spine. These spinal curves in different areas need to be distinguished through localization first during the assessment process. A single spinal curve is encompassed within a local region defined by the three farthest vertebrae, namely, the upper distal vertebra, the lower distal vertebrae, and the apex vertebrae, as illustrated in Figure 1. The localization of a

spinal curve refers to the determination of the positions of the three mentioned key vertebrae. Currently, The Cobb method [4] is the primary measurement technique for assessing spinal curvature. Given that the key idea of the Cobb method is to calculate the angle between the upper endplate of the upper distal vertebra and the lower endplate of the lower distal vertebra or the angle between two straight lines norm to these two endplates respectively, existing works mainly focus on the positioning of the two endplates and completely ignore the position of the curve center (apical vertebrae).

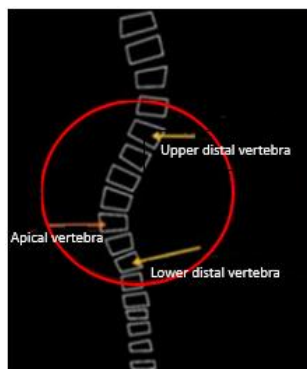


Figure 1. Structural features of a spinal curve

The manual measurement of scoliosis invariably engenders both inter and intra-observer variability [5], [6]. With the assistance of computers, such errors can be significantly reduced [7]. In theory, the less human intervention, the smaller the potential errors. In addition to reducing measurement errors, computer-assisted measurement can also shorten processing time. The automatic localization of the curve is an indispensable and crucial step in automating scoliosis assessment. However, it is a challenging task owing to the following reasons: i) spine images, especially X-rays, are typically low contrast and low image quality, making curve positioning methods based on traditional image processing algorithms ineffective and ii) the inherent complexity of the spinal structure. Firstly, between the spine and the ribs, as well as among adjacent vertebrae within the spine, there is a high degree of similarity. Secondly, the boundaries between the spine and other surrounding tissues, as well as among adjacent vertebrae internally, are not sufficiently clear, particularly in areas where pathology occurs, where the boundaries become even more blurred.

Existing computer-aided measurement methods either rely on manual assistance for localization or entirely give up on localization. Almost none of them discussed the precise localization of the concave center or apex vertebrae. Therefore, this study focuses on the fully automatic localization and distinction of multiple scoliotic curves in the spine on X-rays, with an emphasis on the localization of the centers of each curve. Our contributions are: i) We defined a custom spine central line model to formulate the spine central line as a combination of secant line segments with three possible polarities (positive, negative, and zero) that still retain the trend for the first time; ii) We categorize the curves into 11 types for quick searching and positioning for the first time. Each curve type consists of no more than three consecutive line sequences. The lines in a line sequence have the same polarity but adjacent line sequences have different polarity. Several custom equations are defined to locate curve centers of different curve types; iii) We defined the DTQL algorithm to extract the central line from the extracted spine and group the secant line segments searched from the central line into a series of line sequences with different polarities; and iv) We defined an evaluation criterion adapted from the intersection of union (IoU) to assess the accuracy of curve localization.

This paper consists of five sections. In section 1, the background, motivation, and contributions are discussed. In section 2, the related works are reviewed and analyzed. In section 3, the proposed method is presented. In section 4, the experiments and results are described and analyzed in detail, and a comparison analysis is given about our work and existing related closely articles. Last, the conclusion is presented in section 5.

## 2. RELATED WORKS

According to the definition of the Cobb method, manual measurement of the Cobb angle requires an experienced or trained professional to draw two straight lines on the X-ray film along the edges of the uppermost and lowermost tilted endplates of a spinal curve with a pencil respectively, and then use a

protractor to measure the angle between the two straight lines. Manual measurement not only has low time efficiency (about 20 minutes for a single X-ray film), but also is prone to inter-observer and intra-observer errors due to factors such as operator experience, skill level, and fatigue. Starting from the middle of the last century, experts have been continuously striving to reduce the manual intervention involved in scoliosis measurement. The primary and key problem in the automation of scoliosis measurement is the automatic positioning of the spinal curve.

The earliest computer-assisted measurement methods had a low degree of automation because scoliosis localization relied on manually drawing lines along the target endplates on the screen with a mouse [8], [9], which was inefficient and provided limited assistance in reducing measurement errors. As an improvement, some scholars tried to use a rectangular bounding box to quickly select uppermost and lowermost tilted vertebrae as regions of interest (ROI) and then used image processing algorithms or artificial convolutional neural networks to automatically fit the edge of target endplates in the selected vertebrae. For example, a tailored fuzzy Hough transform [10] algorithm was proposed to fit the edge of target endplates in manually selected ROI in 2009, and a three-layer deep neural network (DNN) model [11] was designed and trained for predicting the slopes of the target endplates in 2017. In this way, the Cobb angle of all curves can be measured and does not require positioning curve centers. However, the rectangular box inevitably selects part of the upper and lower adjacent vertebrae and part of the left and right adjacent tissues when selecting the target vertebrae, which can easily affect the correct edge fitting, especially when the contrast is low or the image contains noise. During the same period, some scholars believed that the measurement of the maximum lateral bend could be used to represent the severity of spinal curvature, so their positioning objective was transferred to the location of the maximum spinal curve. In 2019, a retrained U-net model [12] was used to segment vertebrae first, and then position the uppermost and lowermost endplates of the largest spinal curve by searching the two most tilted lines from up and down edges of all vertebrae's minimum bounding boxes and calculate their intersection angles. However, this method has two potential issues: i) the upper and lower edges of the minimum bounding rectangle may not always be parallel or coincident with the upper and lower edges of the vertebrae and ii) the accuracy of segmentation has a heavy impact on the fitting results.

The angle between two straight lines is equal to the angle between their respective orthogonal lines, which are nearly parallel to or coincide with the spine middle line. Therefore, some scholars attempt to estimate scoliosis by utilizing the spine middle line. One way is to search for the two most tilted straight lines with opposite directions on the spine middle line and take their intersection angle as an approximation of the Cobb angle of the largest curve. In 2002, a human-computer interaction approach [13] was proposed to obtain a spine middle line. In [13], the accuracy of its maximum Cobb angle is related to the number of midline points, which are obtained during human-computer interaction for the construction of the spine middle line, and the quantity of these points can be manually adjusted as needed. To reduce human-computer interaction, a five-layer AlexNet [14] was retrained to predict gravity centers of 17 vertebrae on (Moire, X-ray) image pairs to construct the spine middle line, in 2017. This method involves low manual intervention, requiring only the selection of two reference points on both sides of the shoulder and two points on both sides of the sacrum for aligning the (Moire, X-ray) image pair, and provides a new approach to locate three scoliotic curves based on the trend change of the spine middle line and calculate their Cobb angles. However, it is still semi-automatic and requires multiple image modalities. In 2020, a retrained ResNet50 deep convolutional neuro network (DCNN) [15] was retrained to automatically identify all vertebrae and construct the spine middle line with centers of all vertebrae's bounding boxes, to estimate the Cobb angle of the largest spinal curve. However, not all vertebrae's centroids can coincide with the center points of their bounding rectangular boxes, and the result performance heavily relies on the vertebrae segmentation accuracy. The experimental results also confirmed this inference; among 164 scoliosis cases, 95 cases exhibited an absolute difference greater than 5°.

Some experts choose to train deep convolutional neural networks to directly predict Cobb angles, without focusing on the specific positions of each scoliotic curve. In 2017, a nonlinear classifier named structured support vector regression (S2VR) [16] was defined and trained to jointly estimate Cobb angles and landmarks of the spine in X-rays. S2VR uses relative root mean squared error (RRMSE) and correlation coefficient to assess the performance of Cobb angle estimation and landmark estimation respectively, which achieves a correlation coefficient of 92.76% and the lowest average RRMSE of 21.63. However, S2VR requires preprocessing the X-rays into a uniform size beforehand. With the breakthrough of deep convolutional neuro network in medicine, some authors attempted to design and train DCNN-based models to predict three Cobb angles in X-rays, such as multi-view correlation network (MVC-Net) [17] in 2018 and adaptive error correction network (AEC-Net) [18] in 2019. MVC-Net consists of a landmark estimator and a Cobb angle estimator. The landmark estimator is a custom nonlinear DCNN for predicting landmarks which takes coronal and sagittal X-ray pairs as input, and the Cobb angle estimator is a linear network for estimating three Cobb angles which takes landmarks as input. AEC-Net is similar to MVC-Net in that it also

contains a landmark estimator and Cobb angle estimator, but the structure of the landmark estimator is different from MVC-Net and it takes only a single coronal X-ray image as input. It is worth noting that the mean absolute errors (MAE) of these methods are all less than  $5^\circ$ , and these methods all require input images to have a consistent size. Due to the inherently small size of the dataset and the use of the entire image as the model input, these methods can only employ leave-one-out cross-validation for training. This makes them prone to overfitting, and their generalization ability is yet to be validated. With the purpose of rapid screening, an asymmetry-recognition system [19] using new 3D depth sensor imaging technology was introduced in 2018, which scans the patient's back surface to obtain smoothed, normalized, and tailored 3D point cloud named p3 and its mirror projection named p3r, and calculates the asymmetry index according to the difference between p3 and p3r, which is strongly correlated with the maximum Cobb angle. Reference [20], [21] simplified the procedure of this automated asymmetry-recognition system in 2019 and designed a DCNN-based algorithm in 2021 to take the difference between p3 and p3r as input and predict the maximum Cobb angle directly. The method based on 3D depth sensor imaging is inexpensive, noninvasive, and extremely fast. However, its accuracy for AIS evaluation is 0.94 for the curve of  $\geq 10^\circ$  and 0.89 for the curve of  $\geq 20^\circ$ , not conducive to clinical application. Still, it is a good method for school screening of early spinal deformity.

Not only does scoliosis measurement require the accurate localization and segmentation of spinal structures, but other spinal conditions such as intervertebral disc narrowing and vertebral slippage also demand the localization and segmentation of relevant spinal structures. Therefore, some scholars undertook the study of the localization and segmentation of spinal structures as a research topic. Some of them attempted to locate two to four corners or the center of each vertebra, such as the semi-automatic Harris Corner detector [22] in 2009 and the full-automatic DCNN-based model Boost-Net [23] in 2017. Some of them estimated vertebral centers, such as full-automatic automatic algorithms based on regression forest and probabilistic graphical models [24] in 2012. Some of them attempted to extract the contours of vertebrae or even the whole spine by using shape detection techniques, such as adapted active contour models (ACM) [25]–[29], adapted active shape models (ASM) [30]–[34], adapted level-set method (LSM) [35]–[42], adapted watershed methods (WSM) [43], [44]. Some of them attempted to locate specific parts of vertebrae or vertebral bodies using geometric mathematics and classical image operators, such as custom multiple-feature boundary classification and mesh inflation [45]. Some of them endeavored to train DCNN-based models to segment vertebrae fully automatically [46]–[48]. DCNN-based models achieved a maximum accuracy of 94% dice coefficient, superior to other methods.

Due to the inherent complexity associated with spinal curve localization, some experts have shifted their focus away from conventional Cobb angle measurement. They trained artificial intelligence (AI) based models to classify ROI into several classes directly, such as adapted support vector machine (SVM) to predict whether the observed curve is progressive or non-progressive [49] in 2005 or to categorize curves as mild, moderate, or severe [50] in 2006, fuzzy decision support system (FDSS) [51] to determine whether instrumentation or fusion is warranted. These methods are self-automatic because the location of ROI is identified by hand. Besides, it is noteworthy, that these methods do not possess the capability to precisely locate the spinal curve and consequently offer limited utility in terms of scoliosis monitoring, observation, and treatment planning.

In summary, deep convolutional neural networks make it possible to achieve fully automated measurement of scoliosis with higher accuracy. However, the existing methods are still not mature enough. This paper proposes a custom DTQL-LS model that focuses on automatically distinguishing spinal curves and locating their centers.

### 3. PROPOSED METHOD

The normal human spine is vertically symmetrical with its central axis being a vertical line, but the central axis of the spine with deformity is curved and its curve curvature reflects the severity of scoliosis directly. Thus, the problem of measuring scoliosis can be translated into finding where the spine's central line is curved and measuring its degree of curvature. In this study, we propose a novel fully automatic spinal curve positioning method according to the geometry of the spine's central line. The overall algorithm framework is shown in Figure 2. The proposed model consists of three custom components: i) spine central line model, ii) curve model, and iii) distance transform and quadratic line fitting algorithm coupled with secant line segment searching strategy (DTQL-LS) model. The spine central line model defines a spine central line as a combination of several second-line sequences with different polarities; the curve model classifies all curve shapes into 11 distinct types according to two to three consecutive line sequences with different polarities inside the curve and deduces each curve's concave centers by several custom formulas; and the DTQL-LS model extracts spine central line from the segmented spine by using adapted distance transform first, then formulate it as a secant line sequence obtained through quadratic line fitting strategy, and lastly aggregates adjacent line segments with the same polarity into a line sequence.

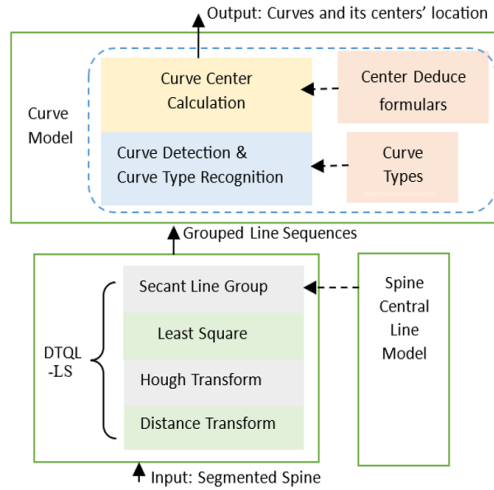


Figure 2. The overall framework of the proposed method

### 3.1. Spine central line model

Our spine central line model describes for the first time the spine central axis as a sequence of secant lines that still retain the trend of the central line. Theoretically, when the distance between any two points on the curve is close enough, the curve segment between the two points can be regarded as a straight line, and a straight line is also a type of curve that represents a special case when tangent and secant lines coincide. As the curvature decreases, the number and length of straight segments that can be found on the curve increases accordingly. Since the central axis of the spine is a vertical straight line except for the local area of the scoliosis center, it is feasible to describe the central axis of the spine with a sequence of secant line vectors.

The basic data unit of our custom central line model is a secant vector which consists of five parameters: i) line polarity, ii) line length, iii) line inclination, iv) line difference between adjacent lines, and v) inclination difference, as shown in Figure 3. The consecutive secant vectors with the same polarity form a line sequence which contains two additional parameters: sequence polarity and sequence distance. The line polarity (LP) has three possible values: positive, negative, and zero, as in (1). A spinal central Line contains n curves (n≤3), as in (2), and each curve is identified by 2 to 3 consecutive line sequences, which will be described in detail later.

$$LP = \begin{cases} \text{Positive,} & \text{if } 0^\circ < \alpha < 90^\circ \\ \text{Negative,} & \text{if } -90^\circ < \alpha < 0^\circ \\ \text{Zero,} & \text{if } \alpha = 90^\circ \end{cases} \quad (1)$$

$$Scl = \text{curve } 1 + \dots + \text{curve } n \quad (2)$$

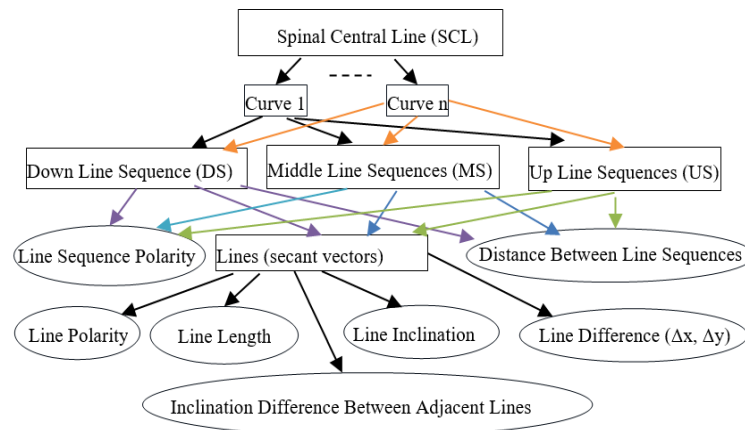


Figure 3. Spinal central line model

**3.2. Curve model**

By analyzing the commonality and specificity of line sequences at different scoliosis locations on spinal central lines, we proposed dividing curves into 11 curve types named T1-T11 respectively for the first time, as shown in Figure 4. To display curve types intuitively, in our curve model, green arrows are used to denote the line sequence with negative angles, brown red arrows are used to denote line sequence with 90° angles and blue arrows are used to denote line sequence with positive angles, as shown in Figures 4(a) to 4(k). If the combination of any three consecutive sequences within the central axis belongs to the categories represented in Figures 4(a) to 4(h), it indicates that the region where these three sequences are located is indicative of a lateral curvature. Figures 4(i) to 4(k) represents three exceptions that may contain spinal curves, and the presence of lateral curvature in the corresponding region may require additional information for further confirmation. The line polarity distributions of different curve types are listed in Table 1.

T1 and T2 have two common features: i) curve contains two sequences: the up sequence (US) and the down sequence (LS) and ii) the sequence LS and US has different directions, one of them is positive and the other is negative, namely,  $L_{\alpha i} \times U_{\beta j} < 0$ . The only difference between these two curve types is that the concave side of type 1 is oriented to the left, and the concave side of type 2 is toward the right, as shown in Figures 4(a) and 4(b), respectively. T3 and T4 are characterized by three distinct parts: a lower sequence, a middle sequence, and an upper sequence, as shown in Figures 4(c) and 4(d). If the middle sequence M is removed, curve type 3 degenerates into type 3, and curve type 4 degenerates into type 1. T5 and T6 all consist of a middle sequence M and an upper sequence U, as shown in Figures 4(e) and 4(f). The only difference is their direction. T7 and T8 contain a lower sequence L and a middle sequence M, as shown in Figures 4(g) and 4(h). T9 and T10 are two exceptions, but similar to type 3 and 4, as shown in Figures 4(i) and 4(j), the only difference is that the lower sequence has the same direction as an upper sequence. T11 is also an exception, with all the line polarities in the central line the same. Figure 4(k) expressed the special case that all line polarities are zero but spinal deformity still existed and can be deduced through deviation of horizontal coordinates between all adjacent line vectors which is named  $\Delta x$  for convenience.

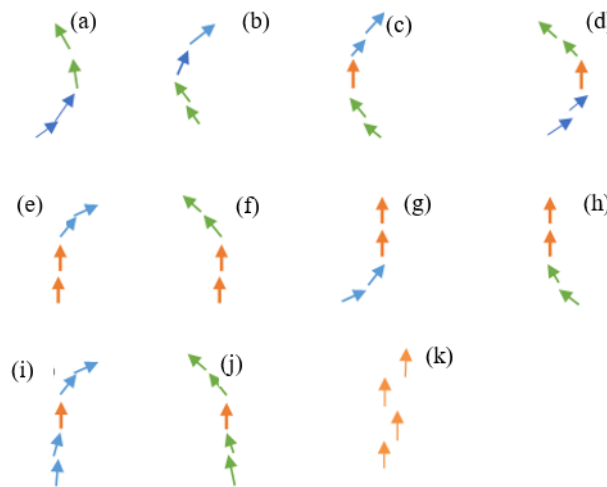


Figure 4. Curve type (a) to (k) representing different line sequence combinations

Table 1. Line sequence polarities of different curve types

Type	Low sequence (LS)	Middle sequence (MS)	Up sequence (US)
T1	Negative	-not exist	Positive
T2	Positive	-not exist	Negative
T3	Positive	Zero	Negative
T4	Negative	Zero	Positive
T5	-not exist	Zero	Negative
T6	-not exist	Zero	Positive
T7	Negative	Zero	-not exist
T8	Positive	Zero	-not exist
T9*	Negative	Zero	Negative
T10*	Positive	Zero	Positive
T11*	All Negative/All Positive/All Zero		

The center of curve type T1 and T2 is typically calculated as in (3), where  $S(c)$  denotes the center of curve  $S$ ,  $(cx, cy)$  denotes the point in  $S$  with minimum or maximum horizontal coordinate value,  $P_x$  denotes the set of horizontal coordinates of all points in  $S$ ,  $(L_{tx}, L_{ty})$  denote the coordinate of the top point in the sequence  $L$ , and  $(U_{bx}, U_{by})$  denotes the coordinate of the bottom point in the sequence  $U$ .

$$S(c) = \begin{cases} (cx, cy) \begin{cases} cx = \min(P_x), \text{ if } S \in T2, \text{ or} \\ cx = \max(P_x), \text{ if } S \in T1 \end{cases}, & \text{if } L_{ty} > cy > U_{by} \\ (cx, cy) \begin{cases} cx = (L_{tx} + U_{bx})/2 \\ cy = (L_{ty} + U_{by})/2 \end{cases}, & \text{elif } U_{by} \leq cy \text{ or } cy \leq L_{ty} \end{cases} \quad (3)$$

The center of T3 or T4 is commonly situated within the middle sequence. If the maximum absolute difference of the X-coordinate differences in sequence  $M$  is less than two, the center is calculated as in (4), where  $(M_{tx}, M_{ty})$  is the coordinate of the top point of  $M$ ,  $(M_{bx}, M_{by})$  is the coordinate of the bottom point of  $M$ ,  $Mx$  is the set of x coordinates, and  $dMx$  is the different sequence of  $Mx$ ,  $l_i$  denotes the  $i$ th line contour in  $M$ , and  $(l_{i_{bx}}, l_{i_{by}})$  denotes the bottom point in  $l_i$ .

$$S(c) = \begin{cases} (cx, cy) \begin{cases} cx = (M_{tx} + M_{bx})/2 \\ cy = (M_{ty} + M_{by})/2 \end{cases}, & \text{if } \max(|dMx|) < 2, \\ (l_{i_{bx}}, l_{i_{by}}), & \text{if } \max(|dMx|) \geq 2 \text{ and } dMx_i * dMx_{i-1} < 0 \\ (cx, cy), \begin{cases} cx = \min(P_x), \text{ if } S \in T3 \\ cx = \max(P_x), \text{ if } S \in T4 \end{cases}, & \text{otherwise} \end{cases} \quad (4)$$

The center of T5 and T6 is usually located at the intersection of these two sequences, and it is calculated as in (5), where  $\|M_t\|$  denotes the length of the top line in  $M$ ,  $d$  is an empirical value, defaulting to 20.

$$S(c) = \begin{cases} (M_{tx}, M_{ty}), & \text{if } \|M_t\| > d, \\ (M_{i_{bx}}, M_{i_{by}}), & \text{if } \max(|dMx|) > 2 \text{ and } dMx_i * dMx_{i-1} < 0, \\ (cx, cy), \begin{cases} cx = \min(M_x \cup U_x), \text{ if } S \in T5 \\ cx = \max(M_x \cup U_x), \text{ if } S \in T6 \end{cases}, & \text{otherwise} \end{cases} \quad (5)$$

The center of T7 and T8 are calculated as in (6), which is similar to (5). The possible center of T9 and T10 is calculated by a slight modification of (4) when it is confirmed that the lateral curvature exists. The concave direction in these types depends on the horizontal deviation between the up sequence, middle sequence, and down sequences.

$$S(c) = \begin{cases} (M_{bx}, M_{by}), & \text{if } \|M_t\| > d, \\ (M_{i_{bx}}, M_{i_{by}}), & \text{if } \max(|dMx|) > 2 \text{ and } dMx_i * dMx_{i-1} < 0, \\ (cx, cy), \begin{cases} cx = \min(L_x \cup M_x), \text{ if } S \in T8 \\ cx = \max(L_x \cup M_x), \text{ if } S \in T7 \end{cases}, & \text{otherwise} \end{cases} \quad (6)$$

The center of T11 is often located within the region exhibiting the maximum horizontal deviation between adjacent lines, which can be calculated as in (7) if the prerequisites are met. In (7),  $l_a$  denotes a sequence of inclination angles of all lines in curve  $S$ ,  $l_{i_a}$  denotes the  $i$ th line angle, and  $dl_a$  denotes the different sequence of  $l_a$ .

$$S(c) = \begin{cases} (l_{i_{bx}}, l_{i_{by}}), & \text{if } \max(|dlx|) > 2 \text{ and } dl_{x_i} * dl_{x_{i-1}} < 0 \\ (l_{i_{tx}}, l_{i_{ty}}), & \text{if } dl_{i_a} = \max(|dl_a|), \text{ and } \max(|l_a|) - \min(|l_a|) \geq d \\ \emptyset, & \text{else} \end{cases} \quad (7)$$

To provide an initial approximation of the curve center's position, it is essential to assess four key indicators: line length, line inclination, difference of line inclination angles, and horizontal deviation between adjacent

lines. However, it is generally unnecessary to compute these indicators for every line within the sequence. Instead, a focused examination of the last two to four lines in the lower sequence, the first two to four lines in the upper sequence, and selecting lines within the middle sequence suffices.

### 3.3. Custom DTQL-LS algorithm

Given the continuous nature of the curve, the quantity of attainable secant lines on its surface is deemed infinite, nevertheless, only a limited number of such lines that can effectively capture the trend in critical regions of lateral curvature are of significance. Therefore, we propose a customized method based on distance transform and quadratic line fitting (DTQL) for extracting and filtering the most optimal trend lines. Our DTQL method utilizes adapted data transform to extract the central line from the spine and applies a quadratic line fitting method combining Hough Transform with Least Square to detect trend line segments in a central line.

#### 3.3.1. Adapted distance transform

The distance transform (DT) is a classical image processing algorithm utilized to calculate the distance between each point of an object and its nearest background point. It was first introduced in [52] in 1980 and has been commonly employed for the extraction of the skeleton or central line inside an object [53]. However, the central axis extraction algorithm based on distance transform tends to generate undesirable bifurcation lines on the extracted central axis. Improvements are essential to ensure that it meets the requirements for obtaining a smooth spine central axis. For ease of description, the image is taken as the sum of three mutually exclusive subsets: object ( $I_o$ ), object edge ( $I_e$ ), and background ( $I_b$ ), as defined in (8).

$$I = I_o + I_e + I_b \quad (8)$$

Our DTQL method begins by generating distance image  $D$  of the same size as image  $I$ . In image  $D$ , all points belonging to  $I_o$  are initialized as -1, all points belonging to  $I_e$  are initialized as 1, and all points belonging to  $I_b$  are initialized as 0, as defined in (9).

$$D(x, y) = \begin{cases} 1, I(x, y) \in I_e \\ 0, I(x, y) \in I_b \\ -1, I(x, y) \in I_o \end{cases} \quad (9)$$

The distance values of points inside the object are updated iteratively by our Algorithm 1, as shown in Figure 5. Instead of using Euclidean distance [54], [55], our adapted DT algorithm determines the distance value of each object point by adding a value of 1 to the smallest non-negative distance value among its eight neighbors. The distance values of those points located at the object center often are local maximum. Henceforth, our algorithm partitions the distance image into slices of three rows each and searches its local maximum. The points with distance values equal to these local maxima are designated as candidate points for the central axis.

Similar to other distance transform algorithms, the central axis formed by points with local maximum distance values exhibits issues such as discontinuity and a relatively wide line (typically up to two pixels wide). As our algorithm employs slices with a height of three, the intervals arising vertically within each slice due to the absence of local maxima do not exceed three. Therefore, the issue of discontinuity can be easily solved by directly connecting adjacent breakpoints. As for the wide central line, just delete one adjacent point with a local maximum on the same line.

#### 3.3.2. Quadratic line fitting

The Hough transform is a widely employed line detection algorithm primarily utilized for the identification of lines within binary image contours. Nevertheless, when applied to skeleton images, it frequently yields an excessive number of shorter line segments, which can impede the accurate localization of curves. Additionally, the proliferation of numerous line segments contributes to an increase in processing time, further compounding the computational complexity of the task.

By merging adjacent short lines with a gap of less than two pixels in the detected Hough line set, the number of Hough lines can be reduced effectively. However, the line contour reconstructed from two discontinuous line segments may be no longer straight and needs fitting a new line, which is settled by least square. The least square method is a commonly employed technique for establishing an approximate mathematical relationship between two variable functions using a data set. In the context of this paper, it is utilized to perform a linear regression fit based on the coordinates of all points within the contour.

```

Algorithm 1: Object Point Distance Updating
Input:  $I, s$ 
Output:  $D$ 
1 Initialization:  $D_o(x, y) \leftarrow -1, D_b(x, y) \leftarrow 0, D_e(x, y) \leftarrow 1, s \leftarrow \{(x, y) | D(x, y) == -1\}$ 
2 while  $s$  is not null do
3    $k = 0$ 
4   while  $k <$  number of  $s$  do
5      $i = s[k][0], j = s[k][1]$ 
6      $neighbour8 = [D[i-1, j-1], D[i-1, j], D[i-1, j+1], D[i, j-1],$ 
7        $D[i, j+1], D[i+1, j-1], D[i+1, j], D[i+1, j+1]]$ 
8     if  $\max(neighbour8) > -1$  then
9        $m = 0$ 
10      while  $m <$   $\text{len}(neighbour8)$  do
11        if  $neighbour8[m] == -1$  then  $neighbour8.pop(m)$ 
12        else  $m = m + 1$ 
13      end
14       $D[i, j] = \min(neighbour8) + 1$ 
15       $s.pop(k)$ 
16    else  $k = k + 1$ 
17  end

```

Figure 5. Pseudocode of the iteratively updating of distance values

Precisely, supposing that the expression for the fitting line is represented as in (10), its approximate form, denoted as (11), is determined such that it minimizes the sum of deviations. In other words, it aims to satisfy the conditions  $\partial M / \partial a = 0$  and  $\partial M / \partial b = 0$ . The determination of the variables 'a' and 'b' that meet these conditions is achieved by solving the corresponding system of differential equations, as illustrated in (12). This process results in the unique determination of 'a' and 'b' values that best fit the data.

$$y = ax + b \quad (10)$$

$$M = \sum_{i=1}^n [y_i - (ax_i + b)]^2 \quad (11)$$

$$\begin{cases} \sum_{i=1}^n y_i x_i = b \sum_{i=1}^n x_i + a \sum_{i=1}^n x_i^2 \\ \sum_{i=1}^n y_i = a \sum_{i=1}^n x_i + nb \end{cases} \quad (12)$$

In practical applications, to enhance processing efficiency, it is possible to expedite the determination of 'a' and 'b' by utilizing the highest and lowest points within a line contour. This streamlined approach offers the advantage of swifter computations without significant detriment to the accuracy of spinal curve localization. It is worth noting that the primary objective in spinal curve localization is to discern the overarching trends of line contours rather than achieving pinpoint accuracy in fitting straight lines.

### 3.3.3. Secant line sequence grouping

The line segments obtained by the DTQL algorithm are sorted according to their vertical coordinates for the sake of searching consecutive line segments with the same polarity and grouping them into a line sequence. After grouping, a spine central line can be viewed as a combination of a series of line sequences with different polarities. What is more, every two or three adjacent line sequences represents a possible spinal curve.

### 3.4. Adapted evaluation criterion

The center of a spinal curve is not a pixel, but an area made up of one or more vertebrae. To assess the accuracy of the curve localization result, the ground truth label should be assigned to each curve center. In this study, the ground truth mark of each curve center is a blue circle to enclose all the vertebrae inside the center area, as shown in Figure 6, and as a contrast, the predicted centers are identified with smaller red circles by our algorithm.

The criterion for successfully detecting the scoliosis center is the existence of an intersection between the ground truth center and the predicted center. In the image processing field, the intersection of two areas can be substituted by a convolution operation. Let rectangle P denote the ground truth mark of a spine curve, the point value inside the circle is marked 1 and the other point value is marked 0; let rectangle I denote the predicted result, its point value inside the red circle is 1 and the other is 0. The convolution results of  $I \times P$  is a new rectangle, with a point value of intersection area equals 1 and the other is 0, as shown in rectangle R. Naturally, the IoU is defined in (13), and the accuracy of concave center detecting is defined in (14).

$$IoU = \sum_{x=1}^L \sum_{y=1}^M \frac{2I(x,y) \times P(x,y)}{I(x,y) + P(x,y)} \quad (13)$$

$$Acc = \frac{\sum_{i=1}^N (\sqrt{\sum_{x=1}^L \sum_{y=1}^M \frac{2I(x,y) \times P(x,y)}{I(x,y) + P(x,y)}})}{N} \quad (14)$$

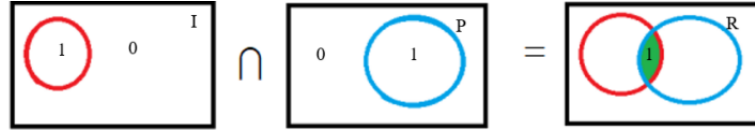


Figure 6. Intersection over union

#### 4. EXPERIMENT AND RESULT DISCUSSION

We developed a fully automatic software system to implement and verify our DTQL-LS-based method. Our spinal curve localization system contains three main modules: spine central line extraction, secant line sequence extraction, and curve localization. The results of these modules will be discussed in detail in section 4.2, 4.3 and 4.4, respectively.

##### 4.1. Data preparation

The spinal X-ray images used in this paper are from the public dataset MICCAI 2019. It contains 609 images of various sizes and quality. Considering that the quality of X-ray images is increasingly improving due to technological advancement, some images in this dataset are no longer suitable for research. To make the proposed method more general and representative, data should be chosen from the dataset according to the following principles: i) the outer contour of the spine must be clear and visible to the naked eye; ii) the contour of the vertebral mass inside the spine is clear and recognizable to the naked eye; iii) various accessories should not appear in spinal X-ray images; iv) exclude images with no side bends or slight side bends that do not require regular observation; and v) exclude spinal images of paralyzed patients or with broken vertebrae.

According to the above five excluding principles, approximately 410 cervicothoracic and 415 thoracolumbar curvatures were selected from 481 images for this experiment. The processing object of this study is the segmented spine by our previous work, which is a transferred semantic segmentation model based on deep convolutional neuro network and will be discussed in another paper in detail. All spinal curve centers in these spines are annotated with blue ellipses. The original spine and its ground truth annotation are shown in Figures 7(a) and 7(b), respectively.

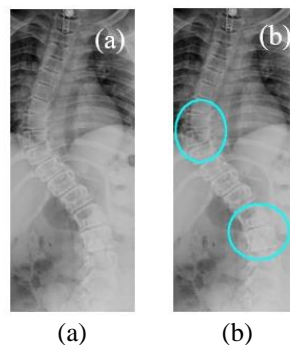


Figure 7. Spine image: (a) original spine and (b) curve center annotated spine

##### 4.2. Spine central line extraction result and comparison

We implemented our adapted DT algorithm on an HP Envy Laptop for central line extraction. To verify its performance, a comparison experiment was conducted between our adapted DT algorithm and OpenCV's built-in DT algorithm. Figure 8 gives an intuitive visual comparison, where Figures 8(a), (b), and (c) represent the original image, the central line extracted by our adapted DT, and the central line extracted by OpenCV's built-in algorithm, respectively. Our algorithm was applied to extract the central axes of the

segmented spine from X-ray images provided by MICCAI 2019, and the results demonstrated that all central axes obtained with our algorithm are free from redundant branching.

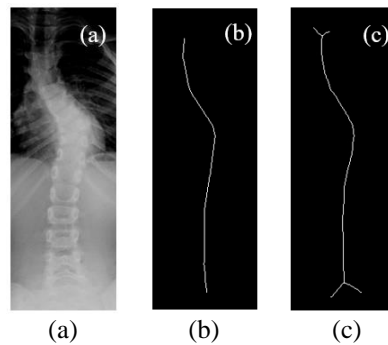


Figure 8. Contrast of central line extraction for (a) original image, (b) central extracted by custom distance transform, and (c) central line extracted by OpenCV's built-in distance transform

#### 4.3. Quadratic line fitting and comparison

We applied our custom quadratic curve fitting method to all spinal central axes. The statistical result showed that our algorithm can reduce the number of secant lines by at least 2 and up to 27 while still preserving the changing trend of the line sequence. Randomly selecting 10 images and numbering them 1-10, the comparison of the number of line segments extracted by our method and the Hough algorithm is shown in Table 2.

Table 2. Result comparison of secant line number

Image number	Line quantity from quadratic line fitting	Line quantity from Hough Line detection
1	24	37
2	27	36
3	21	35
4	23	32
5	27	42
6	18	26
7	29	39
8	22	37
9	24	29
10	27	40

#### 4.4. Curve localization result analysis

We selected 415 thoracolumbar curves and 410 cervicothoracic curves and marked their centers with blue circles as ground truth labels. Statistical results confirmed that 405 out of 410 cervicothoracic curves and 409 out of 415 thoracolumbar curves were successfully detected and finely located, as shown in Table 3. The localization accuracy is close to 99%. Besides, the experiment results proved that our method is time efficient also, it only takes less than 30 milliseconds on average to process X-ray images with different sizes. It has been reported that the computer-assisted semi-automatic measurement method takes approximately 10 minutes to process each X-ray image, with 3 minutes allocated for human-computer interaction. In comparison, the time expenditure of our method for curve localization can be considered negligible. What's more, for some images with blurred boundaries, our program can still identify relatively larger curves.

Figure 9 visually displayed 16 result images illustrating the localization of curve centers. In each image, green lines represent line contours, red circles represent curve centers automatically identified through our method, and the blue ellipses represent the curve centers annotated by hand. Figures 9(a) to 9(k) are X-ray images with relatively high quality, all the curve centers marked by hands were searched out. Figures 9(l) to 9(p) are X-ray images with relatively low quality, and among them, Figure 9(n) represents an image that should be excluded according to our principle. Besides, some curve centers unmarked by hand were also found, as shown in red circles without intersection with blue ellipses in Figures 9(b), 9(d), 9(e), 9(n), and 9(o). Experiments result verified that our algorithm is robust and can locate spinal curves well in images that should have been excluded.

Table 3. Statistical result of spinal curve detection

Scoliosis region	Ground truth centers	Detected centers	Accuracy
Cervicothoracic	410	405	0.99
Thoracolumbar	415	409	0.99

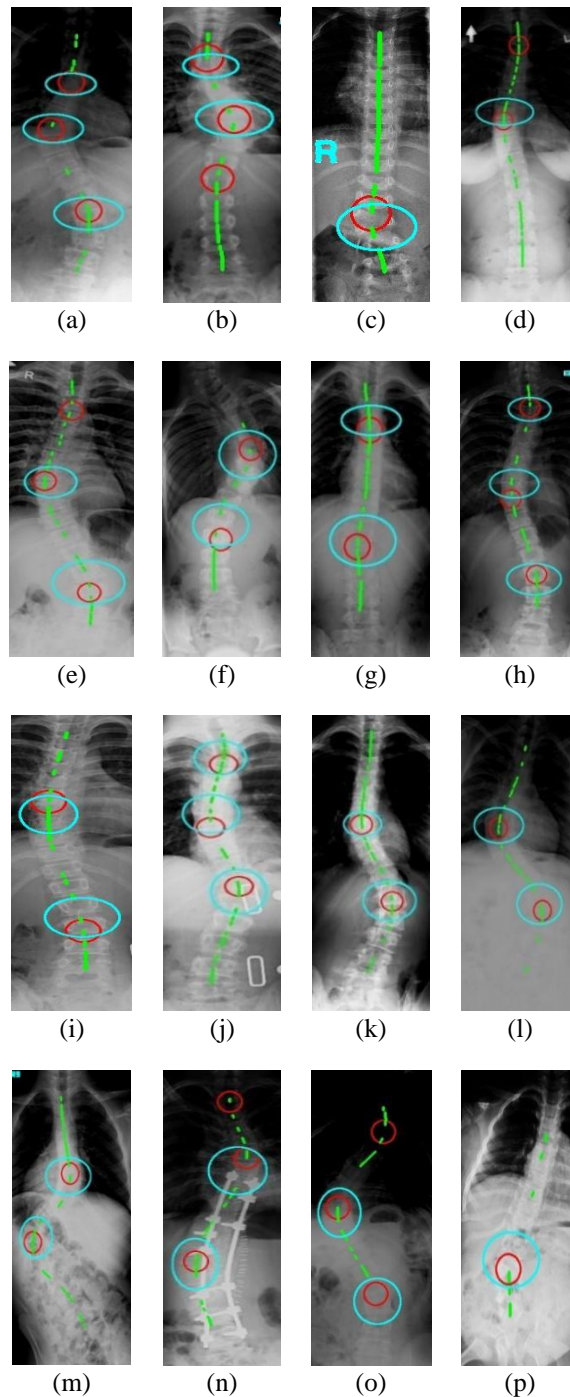


Figure 9. Ground-truth curve centers (marked in blue circle) and predicted curve centers (marked in red circle) in X-ray images (a) to (p)

#### 4.5. Comparison and discussion

Table 4 is a summary of the comparison of 42 articles related to the automated analysis of spinal disorders with our method. It can be seen from Table 4 that our DTQL-LS-based method is the only one to address the problem of localization for different spinal curves and its centers on segmented spine. Besides,

our algorithm is fully-automatic, thoroughly free from manual intervention. Although the initial goal is to locate the spinal curve and its centers, our DTQL-LS-based method also can be used on other occasions where curve localization is required.

Table 4. Comparison of automatic localization in various scoliosis assessment

Index	Automation level	Localization target	Manual operation	Research objective
[10], [11]	Semi-automatic	Upper and lower distal vertebrae of each curve	Mouse draw rectangle	Cobb angles of all curves
[12]	Automatic	Each vertebra and its upper and lower edges	No	Cobb angle of biggest curve
[13]	Semi-automatic	i) 2 ends of a spine and ii) 2 intersection points	Mouse click points	Cobb angle of biggest curve
[14]	Semi-automatic	Tendency changes points	Mouse click 4 reference points	Cobb angle of all curves
[15]	Semi-automatic	Each vertebra and its center	Mouse click alignment point	Cobb angle of all curves
[16]–[18]	Automatic	4 corners of each vertebra	no	Cobb angle of all curves
[19]–[21]	Semi-automatic	Calibrated ROI	Sensor field-of-view calibration manually	Cobb angle of biggest curve
[22]	Semi-automatic	Left 2 corners of each vertebra	Mouse click research center	Vertebral mobility
[23]	Automatic	4 corners of each vertebra	No	Landmark localization
[24]	Automatic	Center of each vertebra	No	Vertebrae localization
[25], [26], [35]–[42], [27]–[34]	Semi-automatic	Contour of vertebrae	Mouse click initial position	Vertebrae segmentation
[43]–[45]	Automatic	Contour of vertebrae	No	Vertebrae segmentation
[46]–[48]	Automatic	Each vertebra	No	Vertebrae segmentation
[49]–[51]	Semi-automatic	ROI	Mouse draw rectangle	Scoliosis level prediction
Ours <sup>*</sup>	Full-automatic	Each curve and its center	No	spinal curve and its center positioning

## 5. CONCLUSION

In this study, we proposed a custom DTQL-LS-based model to differentiate and position different spinal curves and their concave centers from automatically segmented spine. Our method models the spine central line as a combination of line sequences with different polarities while preserving its changing tendency. It categorizes spinal curves into 11 curve types and formulates corresponding empirical formulas to estimate the concave center of each spinal curve. The custom DTQL algorithm consists of adapted distance transform and quadratic fitting for detecting the spine central line from the segmented spine and extracting secant line segments in the spinal central line respectively. We also developed a fully automatic system to implement and verify our DTQL-LS-based model, which contains 3 main modules for spine central line extraction, secant line sequence extraction, and curve localization in turn. The experiment results indicated that our method has agreeable performance with positioning accuracy close to 99%, and has only a slight increase in time overhead (less than 30 milliseconds). Additionally, our algorithm exhibited a certain level of robustness, as it can effectively locate spinal curves in some images that should have been excluded.

## ACKNOWLEDGEMENTS

This work is supported by the Scientific Research Fund of Hunan Provincial Education Department (22A0592) and is also supported by Provincial Natural Science Foundation of Hunan (2023JJ30083). Besides, the author would like to thank Dr. Shi Yuan Quan for providing a deep learning experimental platform, which is the foundation for this work to be carried out.

## REFERENCES

- [1] S. L. Weinstein, L. A. Dolan, J. C. Cheng, A. Danielsson, and J. A. Morcuende, "Adolescent idiopathic scoliosis," *The Lancet*, vol. 371, no. 9623, pp. 1527–1537, May 2008, doi: 10.1016/S0140-6736(08)60658-3.
- [2] F. E. D. Griffiths, "Liver abscess due to foreign-body migration from the alimentary tract a report of two cases," *British Journal of Surgery*, vol. 42, no. 176, pp. 667–668, Dec. 2005, doi: 10.1002/bjs.18004217620.
- [3] R. Wynne-Davies, "Congenital vertebral anomalies: aetiology and relationship to spina bifida cystica," *Journal of Medical Genetics*, vol. 12, no. 3, pp. 280–288, Sep. 1975, doi: 10.1136/jmg.12.3.280.
- [4] J. E. H. Puijts, M. A. P. E. Hageman, W. Keessen, R. van der Meer, and J. C. van Wieringen, "Variation in Cobb angle measurements in scoliosis," *Skeletal Radiology*, vol. 23, no. 7, pp. 517–520, Oct. 1994, doi: 10.1007/BF00223081.
- [5] R. W. Parkinson and P. Hirst, "A simple needle guard for low-volume, high-pressure irrigation," *Injury*, vol. 21, no. 2, Mar. 1990, doi: 10.1016/0020-1383(90)90076-7.
- [6] M. Ogon *et al.*, "Interobserver and intra observer reliability of Lenke's new scoliosis classification system," *Spine*, vol. 27, no. 8, pp. 858–862, 2002.

- [7] K. P. Singer, T. J. Jones, and P. D. Breidahl, "A comparison of radiographic and computer-assisted measurements of thoracic and thoracolumbar sagittal curvature," *Skeletal Radiology*, vol. 19, no. 1, Jan. 1990, doi: 10.1007/BF00197923.
- [8] K. G. Shea, P. M. Stevens, M. Nelson, J. T. Smith, K. S. Masters, and S. Yandow, "A comparison of manual versus computer-assisted radiographic measurement," *Spine*, vol. 23, no. 5, pp. 551–555, 1998, doi: 10.1097/00007632-199803010-00007.
- [9] M. C. Tanure, A. P. Pinheiro, and A. S. Oliveira, "Reliability assessment of Cobb angle measurements using manual and digital methods," *The Spine Journal*, vol. 10, no. 9, pp. 769–774, Sep. 2010, doi: 10.1016/j.spinee.2010.02.020.
- [10] J. Zhang, E. Lou, L. H. Le, D. L. Hill, J. V. Raso, and Y. Wang, "Automatic Cobb measurement of scoliosis based on fuzzy hough transform with vertebral shape prior," *Journal of Digital Imaging*, vol. 22, no. 5, pp. 463–472, Oct. 2009, doi: 10.1007/s10278-008-9127-y.
- [11] J. Zhang, H. Li, L. Lv, and Y. Zhang, "Computer-aided Cobb measurement based on automatic detection of vertebral slopes using deep neural network," *International Journal of Biomedical Imaging*, vol. 2017, pp. 1–6, 2017, doi: 10.1155/2017/9083916.
- [12] M.-H. Horng, C.-P. Kuok, M.-J. Fu, C.-J. Lin, and Y.-N. Sun, "Cobb angle measurement of spine from X-ray images using convolutional neural network," *Computational and Mathematical Methods in Medicine*, vol. 2019, pp. 1–18, Feb. 2019, doi: 10.1155/2019/6357171.
- [13] N. Chockalingam, P. H. Dangerfield, G. Giakas, T. Cochrane, and J. C. Dorgan, "Computer-assisted Cobb measurement of scoliosis," *European Spine Journal*, vol. 11, no. 4, pp. 353–357, Aug. 2002, doi: 10.1007/s00586-002-0386-x.
- [14] R. H. Alharbi, M. B. Alshaye, M. M. Alkanhal, N. M. Alharbi, M. A. Alzahrani, and O. A. Alrehaili, "Deep learning based algorithm for automatic scoliosis angle measurement," in *2020 3rd International Conference on Computer Applications & Information Security (ICCAIS)*, Mar. 2020, pp. 1–5, doi: 10.1109/ICCAIS48893.2020.9096753.
- [15] R. Choi *et al.*, "CNN-based spine and Cobb angle estimator using moire images," *IEEEJ transactions on image electronics and visual computing*, vol. 5, no. 2, pp. 135–144, 2017.
- [16] H. Sun, X. Zhen, C. Bailey, P. Rasoulinejad, Y. Yin, and S. Li, "Direct estimation of spinal cobb angles by structured multi-output regression," *International conference on information processing in medical imaging*, pp. 529–540, 2017.
- [17] H. Wu, C. Bailey, P. Rasoulinejad, and S. Li, "Automated comprehensive Adolescent Idiopathic Scoliosis assessment using MVC-Net," *Medical Image Analysis*, vol. 48, pp. 1–11, Aug. 2018, doi: 10.1016/j.media.2018.05.005.
- [18] B. Chen, Q. Xu, L. Wang, S. Leung, J. Chung, and S. Li, "An automated and accurate spine curve analysis system," *IEEE Access*, vol. 7, pp. 124596–124605, 2019, doi: 10.1109/ACCESS.2019.2938402.
- [19] H. Sudo *et al.*, "Automated noninvasive detection of idiopathic scoliosis in children and adolescents: a principle validation study," *Scientific Reports*, vol. 8, no. 1, Dec. 2018, doi: 10.1038/s41598-018-36360-w.
- [20] T. Kokabu *et al.*, "Three-dimensional depth sensor imaging to identify adolescent idiopathic scoliosis: a prospective multicenter cohort study," *Scientific Reports*, vol. 9, no. 1, Jul. 2019, doi: 10.1038/s41598-019-46246-0.
- [21] T. Kokabu *et al.*, "An algorithm for using deep learning convolutional neural networks with three dimensional depth sensor imaging in scoliosis detection," *The Spine Journal*, vol. 21, no. 6, pp. 980–987, Jun. 2021, doi: 10.1016/j.spinee.2021.01.022.
- [22] M. Benjelloun and S. Mahmoudi, "Spine localization in X-ray images using interest point detection," *Journal of Digital Imaging*, vol. 22, no. 3, pp. 309–318, Jun. 2009, doi: 10.1007/s10278-007-9099-3.
- [23] H. Wu, C. Bailey, P. Rasoulinejad, and S. Li, "Automatic Landmark estimation for adolescent idiopathic scoliosis assessment using BoostNet," *Medical Image Computing and Computer Assisted Intervention – MICCAI 2017. Lecture Notes in Computer Science*, vol. 10433. Springer, Cham. 2017, pp. 127–135, doi: 10.1007/978-3-319-66182-7\_15.
- [24] B. Glocker, J. Feulner, A. Criminisi, D. R. Haynor, and E. Konukoglu, "Automatic localization and identification of vertebrae in arbitrary field-of-view CT scans," *Medical Image Computing and Computer-Assisted Intervention - MICCAI 2012, 2012*, pp. 590–598, doi: 10.1007/978-3-642-33454-2\_73.
- [25] C. Kauffmann and J. A. de Guise, "Digital radiography segmentation of a scoliotic vertebral body using deformable models," *Proceedings of the SPIE*, Apr. 1997, pp. 243–251, doi: 10.1117/12.274114.
- [26] Yalin Zheng, M. S. Nixon, and R. Allen, "Automatic lumbar vertebrae segmentation in fluoroscopic images via optimised concurrent Hough transform," in *2001 Conference Proceedings of the 23rd Annual International Conference of the IEEE Engineering in Medicine and Biology Society*, 2001, vol. 3, pp. 2653–2656, doi: 10.1109/IEMBS.2001.1017328.
- [27] A. Tezmoz, H. Sari-Sarraf, S. Mitra, R. Long, and A. Gururajan, "Customized Hough transform for robust segmentation of cervical vertebrae from X-ray images," in *Proceedings Fifth IEEE Southwest Symposium on Image Analysis and Interpretation*, 2002, pp. 224–228, doi: 10.1109/IAI.2002.999922.
- [28] M. A. Larham, S. Mahmoudi, and M. Benjelloun, "Semi-automatic detection of cervical vertebrae in X-ray images using generalized hough transform," in *2012 3rd International Conference on Image Processing Theory, Tools and Applications (IPTA)*, Oct. 2012, pp. 396–401, doi: 10.1109/IPTA.2012.6469570.
- [29] M. A. Larham, M. Benjelloun, and S. Mahmoudi, "Vertebra identification using template matching modelmp and K K-means clustering," *International Journal of Computer Assisted Radiology and Surgery*, vol. 9, no. 2, pp. 177–187, Mar. 2014, doi: 10.1007/s11548-013-0927-2.
- [30] L. R. Long and G. R. Thoma, "Use of shape models to search digitized spine X-rays," in *Proceedings 13th IEEE Symposium on Computer-Based Medical Systems. CBMS 2000*, 2000, pp. 255–260, doi: 10.1109/CBMS.2000.856908.
- [31] S. Allen, E. Parent, M. Khorasani, D. L. Hill, E. Lou, and J. V. Raso, "Validity and reliability of active shape models for the estimation of Cobb angle in patients with adolescent idiopathic scoliosis," *Journal of Digital Imaging*, vol. 21, no. 2, pp. 208–218, Jun. 2008, doi: 10.1007/s10278-007-9026-7.
- [32] M. Benjelloun, S. Mahmoudi, and F. Lecron, "A framework of vertebra segmentation using the active shape model-based approach," *International Journal of Biomedical Imaging*, vol. 2011, pp. 1–14, 2011, doi: 10.1155/2011/621905.
- [33] B. Ibragimov, B. Likar, F. Pernus, and T. Vrtovec, "Shape representation for efficient landmark-based segmentation in 3-D," *IEEE Transactions on Medical Imaging*, vol. 33, no. 4, pp. 861–874, Apr. 2014, doi: 10.1109/TMI.2013.2296976.
- [34] J. Ma and L. Lu, "Hierarchical segmentation and identification of thoracic vertebra using learning-based edge detection and coarse-to-fine deformable model," *Computer Vision and Image Understanding*, vol. 117, no. 9, pp. 1072–1083, Sep. 2013, doi: 10.1016/j.cviu.2012.11.016.
- [35] S. Tan, J. Yao, M. Ward, L. Yao, and R. Summers, "3D Multi-scale level set segmentation of vertebrae," in *2007 4th IEEE International Symposium on Biomedical Imaging: From Nano to Macro*, 2007, pp. 896–899, doi: 10.1109/ISBI.2007.356997.
- [36] P. H. Lim, U. Bagci, and L. Bai, "Introducing Willmore flow into level set segmentation of spinal vertebrae," *IEEE Transactions on Biomedical Engineering*, vol. 60, no. 1, pp. 115–122, Jan. 2013, doi: 10.1109/TBME.2012.2225833.
- [37] J. Huang, F. Jian, H. Wu, and H. Li, "An improved level set method for vertebra CT image segmentation," *BioMedical Engineering OnLine*, vol. 12, no. 1, Dec. 2013, doi: 10.1186/1475-925X-12-48.
- [38] S. Ruiz-Espana, A. Diaz-Parra, E. Arana, and D. Moratal, "A fully automated level-set based segmentation method of thoracic and lumbar vertebral bodies in Computed Tomography images," in *2015 37th Annual International Conference of the IEEE*

- Engineering in Medicine and Biology Society (EMBC)*, Aug. 2015, pp. 3049–3052, doi: 10.1109/EMBC.2015.7319035.
- [39] Y. Li, W. Liang, Y. Zhang, and J. Tan, “Automatic global level set approach for lumbar vertebrae CT image segmentation,” *BioMed Research International*, vol. 2018, pp. 1–12, Oct. 2018, doi: 10.1155/2018/6319879.
- [40] F. Rehman, S. I. Ali Shah, N. Riaz, and S. O. Gilani, “A robust scheme of vertebrae segmentation for medical diagnosis,” *IEEE Access*, vol. 7, pp. 120387–120398, 2019, doi: 10.1109/ACCESS.2019.2936492.
- [41] F. Rehman, S. I. Ali Shah, M. N. Riaz, S. O. Gilani, and Faiza R., “A region-based deep level set formulation for vertebral bone segmentation of osteoporotic fractures,” *Journal of Digital Imaging*, vol. 33, no. 1, pp. 191–203, Feb. 2020, doi: 10.1007/s10278-019-00216-0.
- [42] K. A. Patil and K. V. M. Prashant, “Segmentation of Lumbar [L1-L4] AP spine X-ray images using various level set methods to detect osteoporosis,” in *2021 IEEE Bombay Section Signature Conference (IBSSC)*, Nov. 2021, pp. 1–6, doi: 10.1109/IBSSC53889.2021.9673249.
- [43] J. Yao, S. D. O’Connor, and R. M. Summers, “Automated spinal column extraction and partitioning,” in *3rd IEEE International Symposium on Biomedical Imaging: Macro to Nano*, 2006, pp. 390–393, doi: 10.1109/ISBI.2006.1624935.
- [44] C. Chevrefils, F. Chériet, G. Grimard, and C.-E. Aubin, “Watershed segmentation of intervertebral disk and spinal canal from MRI images,” in *Image Analysis and Recognition*, Berlin, Heidelberg: Springer Berlin Heidelberg, 2007, pp. 1017–1027.
- [45] D. Zukic *et al.*, “Segmentation of vertebral bodies in MR images,” *Vision, Modeling, and Visualization*, pp. 135–142, 2012, doi: 10.2312/PE.VMV.VMV12.
- [46] M. Vania, D. Mureja, and D. Lee, “Automatic spine segmentation from CT images using convolutional neural network via redundant generation of class labels,” *Journal of Computational Design and Engineering*, vol. 6, no. 2, pp. 224–232, Apr. 2019, doi: 10.1016/j.jcde.2018.05.002.
- [47] Y. Hong, B. Wei, Z. Han, X. Li, Y. Zheng, and S. Li, “MMCL-Net: spinal disease diagnosis in global mode using progressive multi-task joint learning,” *Neurocomputing*, vol. 399, pp. 307–316, Jul. 2020, doi: 10.1016/j.neucom.2020.01.112.
- [48] Z. Han, B. Wei, X. Xi, B. Chen, Y. Yin, and S. Li, “Unifying neural learning and symbolic reasoning for spinal medical report generation,” *Medical Image Analysis*, vol. 67, Jan. 2021, doi: 10.1016/j.media.2020.101872.
- [49] P. O. Ajemba, L. Ramirez, N. G. Durdle, D. L. Hill, and V. J. Raso, “A support vectors classifier approach to predicting the risk of progression of adolescent idiopathic scoliosis,” *IEEE Transactions on Information Technology in Biomedicine*, vol. 9, no. 2, pp. 276–282, Jun. 2005, doi: 10.1109/TITB.2005.847169.
- [50] L. Ramirez, N. G. Durdle, V. J. Raso, and D. L. Hill, “A support vector machines classifier to assess the severity of idiopathic scoliosis from surface topography,” *IEEE Transactions on Information Technology in Biomedicine*, vol. 10, no. 1, pp. 84–91, Jan. 2006, doi: 10.1109/TITB.2005.855526.
- [51] M.-L. Nault, H. Labelle, C.-É. Aubin, and M. Balazinski, “The use of fuzzy logic to select which curves need to be instrumented and fused in adolescent idiopathic scoliosis: a feasibility study,” *Journal of Spinal Disorders & Techniques*, vol. 20, no. 8, pp. 594–603, Dec. 2007, doi: 10.1097/BSD.0b013e318046eb30.
- [52] P.-E. Danielsson, “Euclidean distance mapping,” *Computer Graphics and Image Processing*, vol. 14, no. 3, pp. 227–248, Nov. 1980, doi: 10.1016/0146-664X(80)90054-4.
- [53] C. W. Niblack, P. B. Gibbons, and D. W. Capson, “Generating skeletons and centerlines from the distance transform,” *CVGIP: Graphical Models and Image Processing*, vol. 54, no. 5, pp. 420–437, Sep. 1992, doi: 10.1016/1049-9652(92)90026-T.
- [54] G. Borgefors, “Distance transformations in digital images,” *Computer Vision, Graphics, and Image Processing*, vol. 34, no. 3, pp. 344–371, Jun. 1986, doi: 10.1016/S0734-189X(86)80047-0.
- [55] G. J. Grevera, “Distance transform algorithms and their implementation and evaluation,” in *Deformable Models*, New York, NY: Springer New York, 2007, pp. 33–60.

## BIOGRAPHIES OF AUTHORS



**Aishu Xie**     is a lecturer at the Faculty of Computer and Artificial Intelligence, at Huaihua University. Her research interest generally falls under medical image processing, artificial intelligence, and mathematical modeling. She received her bachelor of biology education from Southwest University in 1996, and her master of computer science and technology from Hunan University in 2009, respectively. She is currently studying for a PhD at the Faculty of Computing and Informatics, University Malaysia Sabah. She can be contacted at email: aishushuxie@sina.com.



**Ervin Gubin Moug**     is a senior lecturer in the Faculty of Computing and Informatics, Universiti Malaysia Sabah. His research interest generally falls under computer vision and pattern recognition, such as image processing, image segmentation, image classification, object detection, vision-based learning, and big data analytics. His domain of interest includes public health, smart health, agriculture, food security, biodiversity, and environmental sustainability. He received his Bachelor of Computer Engineering, master of (computer) engineering, and Ph.D. in computer engineering from Universiti Malaysia Sabah (UMS) in 2008, 2013, and 2018, respectively. He can be contacted at: ervin@ums.edu.my.



**Xu Zhou**    received a master's degree from the Department of Information Science and Engineering, Hunan University, in 2009. She is currently a professor in the Department of Information Science and Engineering, at Hunan University, Changsha, China. Her research interests include parallel computing and data management. She can be contacted at email: zhxu@hnu.edu.cn.



**Zhibang Yang**    received a PhD degree in computer science from Hunan University, Changsha, China, in 2012. He is currently a professor at Changsha University. His major research contains data management and parallel computing. He can be contacted at email: yangzb@ccsu.edu.cn.